Journal of Astronomical Telescopes, Instruments, and Systems

AstronomicalTelescopes.SPIEDigitalLibrary.org

Thermal analyses for initial operations of the soft x-ray spectrometer onboard the Hitomi satellite

Hirofumi Noda
Kazuhisa Mitsuda
Atsushi Okamoto
Yuichiro Ezoe
Kumi Ishikawa
Ryuichi Fujimoto
Noriko Yamasaki
Yoh Takei
Takaya Ohashi
Yoshitaka Ishisaki
Ikuyuki Mitsuishi
Seiji Yoshida
Michel DiPirro
Peter Shirron

Hirofumi Noda, Kazuhisa Mitsuda, Atsushi Okamoto, Yuichiro Ezoe, Kumi Ishikawa, Ryuichi Fujimoto, Noriko Yamasaki, Yoh Takei, Takaya Ohashi, Yoshitaka Ishisaki, Ikuyuki Mitsuishi, Seiji Yoshida, Michel DiPirro, Peter Shirron, "Thermal analyses for initial operations of the soft x-ray spectrometer onboard the Hitomi satellite," *J. Astron. Telesc. Instrum. Syst.* **4**(1), 011202 (2017), doi: 10.1117/1.JATIS.4.1.011202.

SPIE.

Thermal analyses for initial operations of the soft x-ray spectrometer onboard the Hitomi satellite

Hirofumi Noda,[a,b,*] Kazuhisa Mitsuda,[c] Atsushi Okamoto,[d] Yuichiro Ezoe,[e] Kumi Ishikawa,[c] Ryuichi Fujimoto,[f] Noriko Yamasaki,[c] Yoh Takei,[c] Takaya Ohashi,[e] Yoshitaka Ishisaki,[e] Ikuyuki Mitsuishi,[g] Seiji Yoshida,[h] Michel DiPirro,[i] and Peter Shirron[i]

[a]Tohoku University, Frontier Research Institute for Interdisciplinary Sciences, Sendai, Miyagi, Japan
[b]Tohoku University, Astronomical Institute, Sendai, Miyagi, Japan
[c]Institute of Space and Astronautical Science, Japan Aerospace Exploration Agency, Sagamihara, Kanagawa, Japan
[d]Japan Aerospace Exploration Agency, Research and Development Directorate, Tsukuba, Ibaraki, Japan
[e]Tokyo Metropolitan University, Department of Physics, Hachioji, Tokyo, Japan
[f]Kanazawa University, Faculty of Mathematics and Physics, Kanazawa, Ishikawa, Japan
[g]Nagoya University, Department of Physics, Nagoya, Aichi, Japan
[h]Sumitomo Heavy Industries, Ltd., Niihama, Ehime, Japan
[i]National Aeronautics and Space Administration, Goddard Space Flight Center, Greenbelt, Maryland, United States

Abstract. The soft x-ray spectrometer (SXS) onboard the Hitomi satellite achieved a high-energy resolution of ~4.9 eV at 6 keV with an x-ray microcalorimeter array cooled to 50 mK. The cooling system utilizes liquid helium, confined in zero gravity by means of a porous plug (PP) phase separator. For the PP to function, the helium temperature must be kept lower than the λ point of 2.17 K in orbit. To determine the maximum allowable helium temperature at launch, taking into account the uncertainties in both the final ground operations and initial operation in orbit, we constructed a thermal mathematical model of the SXS dewar and PP vent and carried out time-series thermal simulations. Based on the results, the maximum allowable helium temperature at launch was set at 1.7 K. We also conducted a transient thermal calculation using the actual temperatures at launch as initial conditions to determine flow and cooling rates in orbit. From this, the equilibrium helium mass flow rate was estimated to be ~34 to 42 μg/s, and the lifetime of the helium mode was predicted to be ~3.9 to 4.7 years. This paper describes the thermal model and presents simulation results and comparisons with temperatures measured in the orbit. *© The Authors. Published by SPIE under a Creative Commons Attribution 3.0 Unported License. Distribution or reproduction of this work in whole or in part requires full attribution of the original publication, including its DOI.* [DOI: 10.1117/1.JATIS.4.1.011202]

Keywords: Hitomi (ASTRO-H); soft x-ray spectrometer; x-ray microcalorimeter; cryogenics; thermal mathematical model; thermal simulation.

Paper 17015SSP received Apr. 16, 2017; accepted for publication Oct. 3, 2017; published online Oct. 27, 2017.

1 Introduction

The soft x-ray spectrometer (SXS)[1] is an x-ray microcalorimeter array onboard the Japanese x-ray satellite Hitomi (ASTRO-H),[2] which was successfully launched on February 17, 2016, by an H2A rocket from Tanegashima Space Center. Until the end of operations on March 26, 2016, the SXS successfully achieved an unprecedentedly high-energy resolution of ~4.9 eV at 6 keV in orbit at an altitude of 575 km.[2,3] The performance is achieved by cooling the x-ray microcalorimeter array to 50 mK with a cooling system that utilizes a dewar cooled down by several mechanical coolers, adiabatic demagnetization refrigerators (ADRs), and superfluid liquid helium (LHe).

In the cooling system of the SXS,[4] the two-stage Stirling Shield Coolers (SCs) cool from ~300 K to a base temperature of ~20 K, and subsequently, the ^{4}He Joule–Thomson (JT) cooler produces ~4 K. In the case when LHe is present, the venting helium (He) vapor assists in cooling the radiation shields inside the dewar. As a result, the LHe can be kept at ~1.1 K. Finally, two ADR stages operate to stabilize the temperature of the x-ray microcalorimeter array at 50 mK, requiring periodic recycles about once per two days. In the He vent system, a porous plug (PP) phase separator[5,6] is employed to separate liquid and boiloff He in zero gravity, so that only the boiloff He gas is released. Because the PP works only when the LHe is in the superfluid phase, the LHe temperature must always be kept lower than the λ point of LHe. Hence, it is critical that the LHe is launched at a low enough temperature that it cannot exceed the λ point in orbit.

After the final top-off operation before launch, the LHe is pumped to cool to ~1.3 K with the mechanical coolers operating. Before the countdown sequence starts, the pumping is stopped, and the external plumbing is removed. During the countdown sequence, the following procedures are performed: (1) operation of the SCs continues without the JT cooling and vapor cooling of the shields, (2) during rocket roll-out and before the launch, all cryocoolers are powered off. After launch, while the satellite is still under acceleration, (3) the He vent valve is opened, and vapor cooling begins. Finally, (4) after a few orbits, the cryocoolers are powered on. Until this last operation, the heat load on the liquid continues to rise along with the shield temperatures, but afterward, the heat loads decrease and the LHe temperature eventually peaks and starts decreasing. To set the launch hold condition properly, it is critical to estimate the maximum LHe temperature in orbit based on a realistic timeline of pre- and postlaunch operations. For that purpose, we constructed a thermal mathematical model of the SXS

*Address all correspondence to: Hirofumi Noda, E-mail: hirofumi.noda@astr.tohoku.ac.jp

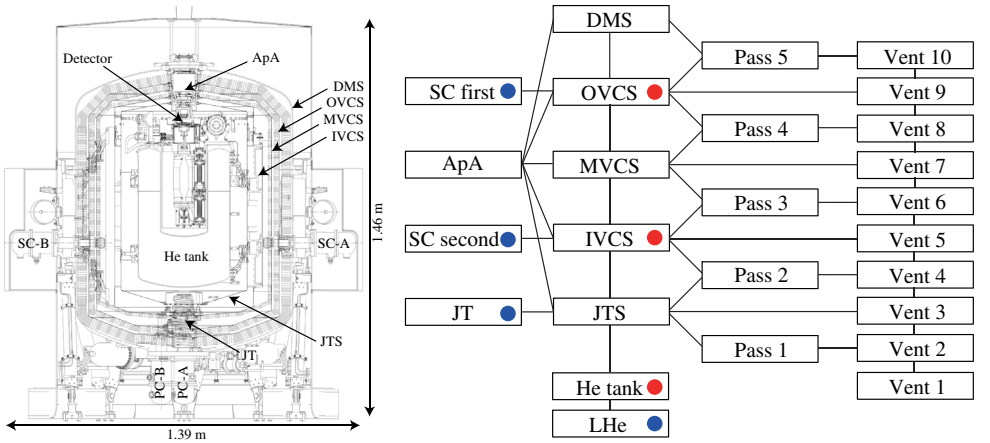

Fig. 1 (a) A cross-sectional view of the SXS Dewar and (b) the schematic structure of the thermal mathematical model of the SXS dewar. Each box represents a node except for the ApA, and solid lines show thermal connections by K_C and/or K_R. Red and blue filled circles show positive (Table 1) and negative heat loads (Table 2), respectively.

dewar and performed numerical thermal simulations during and after steps 3 and 4. For the simulations, we employed the thermal analysis software SINDA/FLUINT version 5.8, which solves heat conduction equations by the finite difference/element method.

2 SXS Thermal Mathematical Model

2.1 *Model Structure*

Figure 1 shows the structure of the SXS dewar. Within the SXS dewar main-shell (DMS) are four aluminum shields, from warmest to coldest these are an outer vapor-cooled shield (OVCS), a middle vapor-cooled shield (MVCS), an inner vapor-cooled shield (IVCS), and a Joule–Thomson shield (JTS). The OVCS and IVCS are cooled by the first and second stages of the two SCs, respectively, while the JTS is cooled by the JT. The MVCS is not actively cooled, but all shields are connected to the He vent line so that they are cooled by the He vapor venting from the He tank. The He tank is suspended from the IVCS using carbon-fiber reinforced plastic straps while the IVCS is suspended from the DMS using glass-fiber reinforced plastic straps. Other shields are also supported by blocks bonded to these straps.[7] Note that the amount of LHe was 35.6 L at the launch.

The dewar thermal structure is modeled as shown in Fig. 1. The shields, He tank, cryocooler stages, and the LHe are each represented by one node, thus ignoring nonuniformity of temperature and heat distribution. Heat capacities of the LHe and the shields are provided as a function of their temperatures. The He tank itself is not explicitly included as its heat capacity is orders of magnitude smaller than that of the LHe. Because the He vent line is connected to the He tank at a point and to the shields at nine points, we utilize 10 nodes to model the He vent line. Reflecting the structure of the support strap, four of the nine nodes are directly connected to the shield nodes, whereas the others are via nodes of pass points as shown in Fig. 1. The vapor cooling is modeled as heat transfer due to boiloff He along the vent line from the He tank to the outside, using one-way conductance among the vent line nodes. Conductive and radiative thermal conductances are defined between connected nodes, and they are denoted by K_C and K_R, respectively. While K_C is determined by the size, material, and the temperature of the conductive paths, K_R depends on the area and the effective emissivity of the surface and multilayer insulations (MLIs). In the determinations of K_R, the effective emissivity at IVCS–JTS and JTS–He tank is fixed at 0.03 while we allow those at DMS–OVCS, OVCS–MVCS, and MVCS–IVCS to differ from 0.03 for temperature adjustment as shown in Sec. 2.3. Note that the aperture assembly (ApA) is only weakly coupled to the DMS and the shields as shown in Fig. 1, and its contribution is not significant.

2.2 *Modeling Heat Generations and Coolings by He and Cryocoolers*

Positive heat loads are input to the He tank from the ADRs (magnets, salt pills, and getter heaters) and the detector assembly (DA). Furthermore, heat conducts to the He tank through mounting structures and through off heat switches 3 and 4 (HS 3/4) from the third ADR to the He tank and JTS, respectively. Joule heatings due to magnet currents through the resistive leads dissipate at the IVCS and OVCS. The heat load from the JFET amplifiers through the harness between the IVCS and the DA is also input to the IVCS. This varies with the IVCS temperature and becomes 0.21 mW when the IVCS is at 24.5 K. [7] We model these positive heat loads at the He tank, IVCS, and OVCS, as shown in Fig. 1 as red circles and summarized in Table 1. Although the heat loads by the ADRs and the lead Joule heatings are actually time variable, they are represented by their time-averaged values. The ADR heat loads shown in Table 1 assume ~1 day interval between recycles. In orbit, the ADR recycle period was actually ~2 days, resulting in a smaller heat load than shown in Table 1 (see Ref. 8). The cooling effects at the shields by the cryocoolers and at the He tank by the He vaporization are supplied as negative heat loads as shown in Fig. 1 as blue circles and summarized in Table 2. The nominal cooling powers of the first and second stages of the SCs, and the JT are given as functions of their temperatures, $T_{\mathrm{SC\,first}}$, $T_{\mathrm{SC\,second}}$, and T_{JT}, respectively.[9,10] He tank cooling by He evaporation is equal to the product of the He mass flow rate $\dot{M}_{\mathrm{He}}$ and the LHe latent heat L_{LHe}. In this paper, $\dot{M}_{\mathrm{He}}$ as a function of the He tank temperature was provided by Ezoe et al.[11] based on breadboard

Table 1 Positive heat loads to the He tank, IVCS, and OVCS nodes in units of mW. The ADR heat loads and Joule heatings are time averaged[a].

	ADR magnets	ADR salt pills	ADR getter heaters	HS 3/4	Lead Joule heating	DA
He tank	0.053	0.063	0.008	0.074	—	0.21[b]
IVCS	—	—	—	—	5.5	13
OVCS	—	—	—	—	11.0	—

[a]The heat loads correspond to the ~1 day ADR recycles, which were planned before the launch. Actually, the period of the ADR recycle was ~2 days in the orbit, and the heat loads became smaller (see Ref. 8).
[b]Depends on the IVCS temperature T_{IVCS}, and the value is when $T_{\mathrm{IVCS}} = 24.5$ K.[7]

Table 2 Negative heat loads to the He tank, the first, and second stage of the SCs, and the JT in units of mW.

	SC coolers	JT cooler	He evaporation
He tank	—	—	$-\dot{M}_{\mathrm{He}} L_{\mathrm{LHe}}$[a]
SC first	$-34 T_{\mathrm{SC\,first}} + 2638$ ($T_{\mathrm{SC\,first}} > 78$ K)[b]	—	—
SC second	$-22 T_{\mathrm{SC\,second}} + 283$ ($T_{\mathrm{SC\,second}} > 13$ K)[c]	—	—
JT	—	$2T_{\mathrm{JT}} - 51$ (4.3 K < T_{JT} < 10 K)[d] $T_{\mathrm{JT}} - 40$ ($T_{\mathrm{JT}} > 10$ K)[d]	—

[a]$\dot{M}_{\mathrm{He}}$ is the He mass flow rate, which is two-third of that reported by Ezoe et al.,[11] while L_{LHe} is the LHe latent heat.[12] Both $\dot{M}_{\mathrm{He}}$ and L_{LHe} depend on the He tank temperature.
[b]$T_{\mathrm{SC\,first}}$ is the temperature of the first stage of the SC in units of K. The heat load is 0 mW when $T_{\mathrm{SC\,first}} < 78$ K.
[c]$T_{\mathrm{SC\,second}}$ is the temperature of the second stage of the SC in units of K. The heat load is 0 mW when $T_{\mathrm{SC\,second}} < 13$ K.
[d]T_{JT} is the temperature of the JT in an unit of K. The heat load is 0 mW when $T_{\mathrm{JT}} < 4.3$ K.

model PP tests but including a correction factor of 2/3. Refer to Ezoe et al.[5] for detailed descriptions about the correction factor that is required to reproduce the flight-model PP mass flow rate. L_{LHe} depends only weakly on the LHe temperature.[12] The relation between the LHe temperature T_{LHe} and the heat load to the He tank Q can be written as

$$C_{\mathrm{LHe}} \frac{\mathrm{d}T_{\mathrm{LHe}}}{\mathrm{d}t} = Q - \dot{M}_{\mathrm{He}} L_{\mathrm{LHe}}, \tag{1}$$

where C_{LHe} is the heat capacity of the LHe. Effects of the vapor cooling along the He vent line described in Sec. 2.1 are determined with $\dot{M}_{\mathrm{He}}$.

2.3 *Comparison with Ground Test in Equilibrium*

Because the effective emissivities of MLI blankets are highly dependent on how they are assembled, the values of K_{R} could include uncertainties relatively larger than those of K_{C}. Hence, we needed to tune K_{R} by comparing a simulated temperature distribution with an actual one measured in a ground test. For the comparison, we chose the latest data in the ground test derived on December 22, 2015, 04:14 (UT), in which all temperatures had achieved equilibrium. Table 3 shows the actual temperatures of the He tank, JTS, IVCS, and the OVCS, and their simulated temperatures after tuning K_{R}. The actual temperatures were reproduced by the steady-state simulation within ~15% deviations.

3 Initial Helium Temperature for Launch Hold Condition

3.1 *Allowable Upper Temperature Limit Including Model Uncertainty*

Although the temperatures can be reproduced to within 15% in the steady-state analysis as shown in Sec. 2.3, calculations at temperatures higher than those in the steady state are necessary in a transient analysis, which evaluates the maximum temperature after the launch. Because the LHe needs to be always in the superfluid phase in orbit, we consider that the maximum temperature must be lower than ~2.1 K, which is slightly margined from the λ point. To be conservative, we decided to incorporate a 100% margin on the He tank heat loads when establishing the maximum allowable LHe temperature. At the maximum LHe temperature, Eq. (1) becomes

$$Q = \dot{M}_{\mathrm{He}} L_{\mathrm{LHe}}. \tag{2}$$

If we ignore the effect of the PP and assume for simplicity that the He mass flow rate is given as $\dot{M}_{\mathrm{He}} = G P_{\mathrm{sat}}(T_{\mathrm{LHe}})$, where G is the He flow conductance in the He vent line and $P_{\mathrm{sat}}(T_{\mathrm{LHe}})$ is the saturated vapor pressure of the boiloff He, Eq. (2) becomes

Table 3 Temperature comparisons in equilibrium between the ground test on December 22, 2015, 04:14 (UT) and the steady-state simulation after tuning K_{R}.

	He tank	JTS	IVCS	MVCS	OVCS	DMS
December 22, 2015, 04:14 (UT)	1.24 K	4.4 K	27.3 K	95.7 K	139.3 K	289 K
Thermal simulation	1.10 K	4.3 K	24.7 K	92.9 K	136.9 K	290 K (fixed)

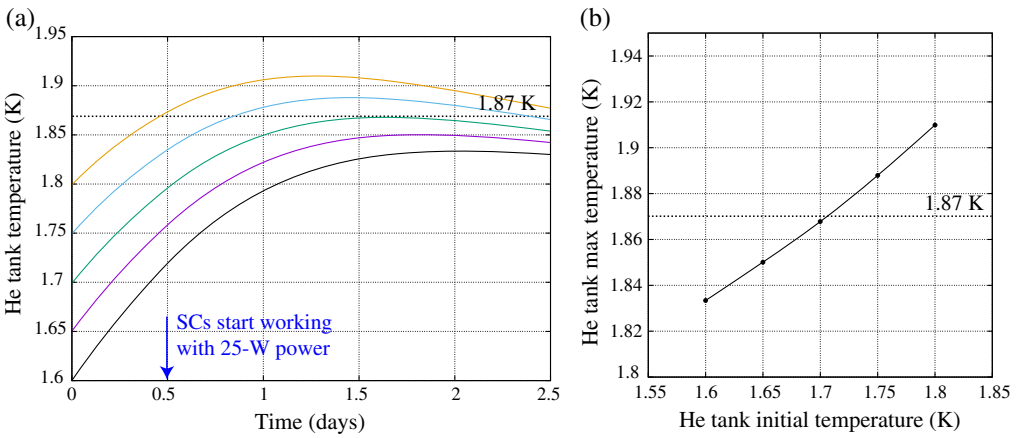

Fig. 2 (a) The simulated temperature variations of the He tank, calculated with various initial temperatures, 1.6 K (black), 1.65 K (magenta), 1.7 K (green), 1.75 K (cyan), and 1.8 K (orange). In the simulations, it was assumed that the SCs start working half a day after the launch with 25-W power. (b) A plot between the initial and maximum He tank temperature.

$$Q = L_{\mathrm{LHe}} G P_{\mathrm{sat}}(T_{\mathrm{LHe}}). \quad (3)$$

Hence, when a 100% margin is added to the heat load corresponding to $T_{\mathrm{LHe}} = 2.1$ K, $L_{\mathrm{LHe}} G P_{\mathrm{sat}}(T_{\mathrm{LHe}})$ needs to be increased by a factor of 2, and the LHe temperature becomes ~1.87 K. Therefore, we set the maximum allowable LHe temperature at 1.87 K.

3.2 *Transient Simulations with Various Initial LHe Temperatures*

With the temperature of the DMS node fixed and initial temperatures of the other nodes set appropriately, we were able to run transient simulations of postlaunch conditions. In the nominal operation plan, the He venting starts ~5 min after launch, and the SC operation with nominal power (50 W × 2) starts ~1 orbit after the He venting begins (procedures 3 and 4 in Sec. 1). But given the possibility that SC startup could be delayed due to unexpected reasons, we carried out simulations by changing not only the initial LHe temperature but also the time to start SC operation. Figure 2(a) shows the LHe temperature variations with the initial temperature at 1.6, 1.65, 1.7, 1.75, and 1.8 K. It was assumed that SC operation starts half a day after the launch, with half the nominal power (25 W × 2). The cooling power of the first and second stages of the SCs by the 25 W × 2 operations is assumed to follow $-20T_{\mathrm{SC\,first}} + 2306$ mW ($T_{\mathrm{SC\,first}} > 113$ K) and $-11\,T_{\mathrm{SC\,second}} + 440$ mW ($T_{\mathrm{SC\,second}} > 38.5$ K), respectively. In all cases, the LHe temperature did not start decreasing immediately after the start of the SC 25-W operations but reached a maximum 1 to 2 days after launch. This is because only the OVCS and IVCS are directly cooled by the SCs, and the He tank temperature responds after the shield temperatures decrease following their time constants. The maximum LHe temperature was lower than 1.87 K, when the initial LHe temperature was 1.7 K but did exceed 1.87 K when the LHe temperature at launch was higher than 1.75 K.

Figure 2(b) shows the relationship between the initial and maximum LHe temperatures, based on the five calculated points. The maximum allowed temperature of 1.87 K was reached when the initial (launch) temperature of the liquid was ~1.704 K. We also conducted a simulation by starting SC operation with nominal power one day after the launch. In this case, the liquid peaked at 1.87 K when the initial temperature was lower, ~1.64 K. Therefore, we adopted 1.7 K as the upper limit of the LHe temperature at launch and required SC operation to start at half the nominal power or higher within 12 h of launch. That shows that the launch would have to be aborted and the helium reconditioned if T_{LHe} exceeded 1.7 K. As shown by Fujimoto et al.,[4] the LHe temperature was ~1.5 K at the final prelaunch decision point, due to careful operations of the SXS team in the procedures 1 and 2 as shown in Sec. 1.

4 Temperature Variations after Launch

4.1 *Temperature Simulations in Orbit*

We conducted a time-series analysis with initial LHe, JTS, IVCS, and OVCS temperatures set at the actual values, i.e., 1.50, 24.6, 41.0, and 158 K, respectively. By radiating in the anti-Sun direction, the DMS cooled to ~260 K,[4] which was ~30 K lower than that on the ground, and hence, we fixed the temperature of the DMS node at 260 K as a boundary. In the analysis, the SC 25-W, SC 50-W, and JT operations started ~3 h, ~4 h, and ~1 day after the launch, following the actual sequence.[13] Figure 3 shows the transient simulation results. The predicted maximum LHe temperature was ~1.53 K, which was below the allowable upper temperature obtained in Sec. 3.2. After peaking at ~1.5 days, the LHe temperature started monotonically decreasing. Similarly, the temperatures of the JTS, IVCS, and the OVCS were predicted to initially increase but then start decreasing several hours after the launch. The simulated temperatures of the LHe, JTS, IVCS, and the OVCS reached equilibrium at ~1.12, ~4.3, ~22, and ~120 K, respectively. All the simulated shield temperatures in equilibrium were lower than those shown in Table 3, presumably because of the lower DMS temperature. The equilibration times for the LHe, JTS, IVCS, and the OVCS temperature were ~20 days, ~1 day, ~5 days, and ~3 days, respectively. Because the shields are directly cooled down by the mechanical coolers and have relatively low heat capacity, they reach equilibrium faster than the LHe.

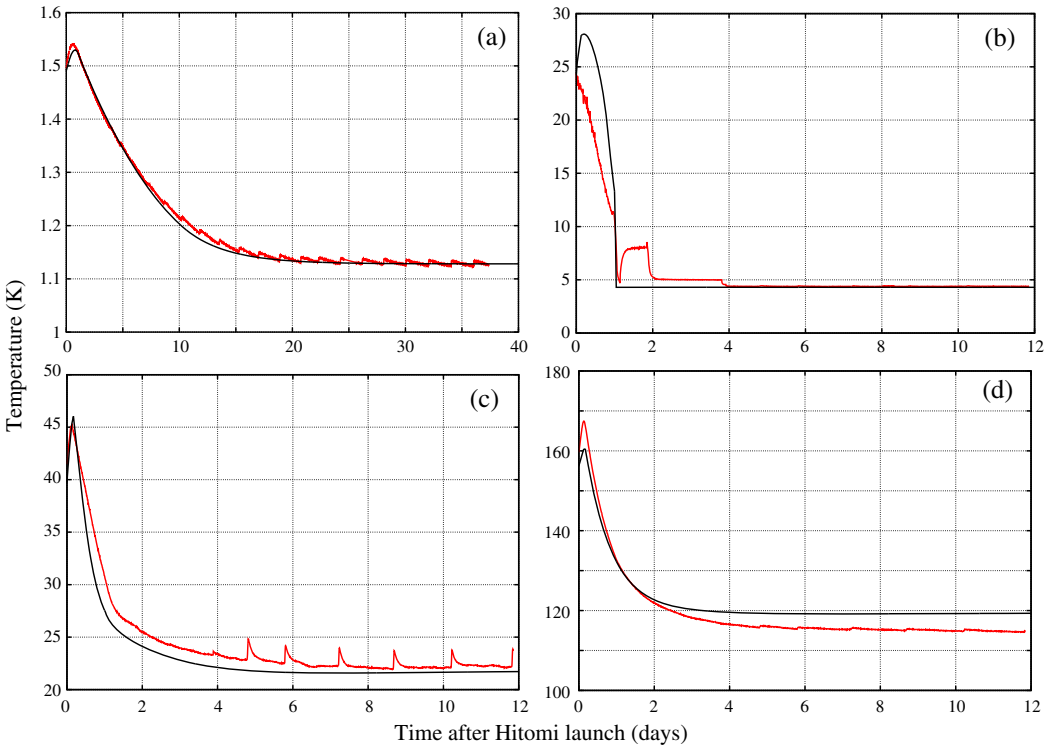

Fig. 3 The simulated (black) and actual (red) temperature variations of (a) the He tank, (b) the JTS, (c) the IVCS, and (d) the OVCS after the Hitomi launch. Panel (b), (c), and (d) show results of the first 12 days in the 40-days calculations and measurements. In the simulation, the initial temperatures were set at the actual values measured at the launch. The positive heat loads to the He tank, IVCS, and the OVCS from the ADRs and current Joule heatings in Table 1 were implemented after being time averaged in the calculation.

4.2 *Comparison between Simulations and Measurements*

In Fig. 3, we superimpose the actual temperature curves of the LHe, JTS, IVCS, and the OVCS measured in the orbit from February 17, 2016, to March 25, 2016,[4,13] and simulation results. The LHe temperature variation was well reproduced by the simulation, except for a few % underestimations at ~0 to 1 days and ~10 to 20 days, and periodic temperature changes that corresponded to the ADR recycles. Note that the positive heat loads of the ADRs were implemented only as time-averaged values, which were updated by orbital measurements. [8] The IVCS and OVCS temperatures were also well reproduced, although deviations of up to 10% were seen. The measured IVCS and OVCS temperatures also showed periodic temperature changes due to the ADR recycles, because the Joule heating by the current leads was larger during the recycles while only the time-averaged heat loads, which were also updated by orbital values,[8] were implemented in the calculations. Note that for days 1 to 4, the actual JTS temperature deviated from the simulation by 1 to 3 K. This is because the JT was turned off autonomously and restarted ~1.1 days and ~1.9 days after the launch, respectively, and then its power was adjusted to fine-tune its operation.[13]

The JTS temperature measured in the orbit decreased monotonically just after He venting started, which is different from the simulation, and the simulation overestimated it by as much as ~20%. The deviation is larger than the uncertainty obtained in Sec. 2.3 (Table 3). This may mean that the simulation cannot accurately reproduce the JTS temperature when it is much higher than its nominal operating temperature (~4.5 K). Possible cause is inaccuracy of the JTS heat capacity in the thermal mathematical model.

4.3 *He Lifetime Estimation*

As described in Sec. 2.2, the He mass flow rate via the PP is calculated as a function of the He tank temperature. Therefore, the model can predict the He mass flow rate and, by integrating, a running total of the vented mass. The results are shown in Fig. 4. The He mass flow rate increased at first, then started decreasing at ~1 day, and reached equilibrium at ~34 μg/s in a few tens days after the launch. The trend is similar to the curve of the simulated He tank temperature as shown in Fig. 3. The amount of He vented in the first few days was consistent with that needed to cool the liquid, and the loss rate eventually stabilized ~20 days after the launch. Figure 4(a) also shows the He mass flow rates estimated from the actual temperatures of the PP and the He tank in the orbit, using the flight-model PP mass flow rate model and two-thirds of that, in order to take the hydrostatic head effect into account.[5] Our prediction is close to the latter in the first ~2 days, but then, coincides with the former very well. Refer to Ezoe et al.[5] for detailed descriptions about the PP mass flow rate model and comparisons with our simulations.

The initial LHe amount was ~35.6 L, which corresponded to ~5162 g. By extrapolating the curve of the consumed LHe in Fig. 4(b) to ~5162 g, the lifetime of the LHe with the

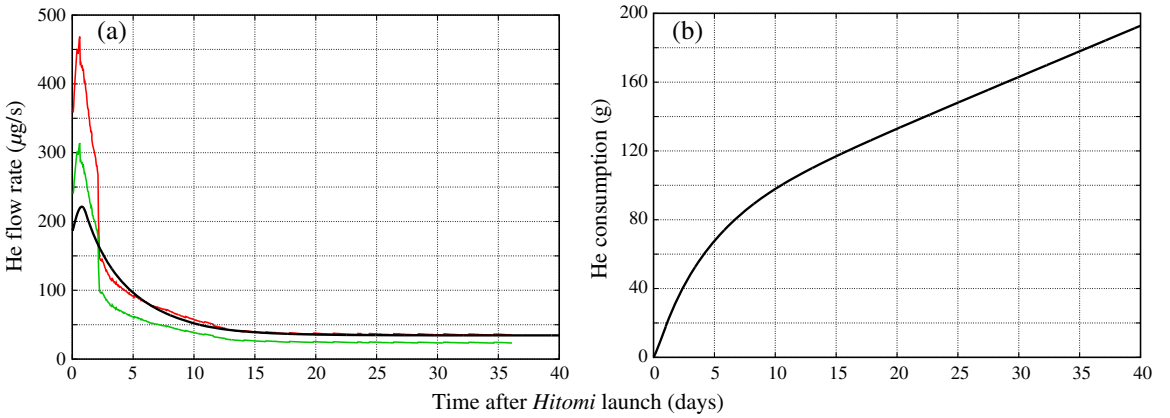

Fig. 4 (a) Black shows the simulated variation of the He mass flow rate. Red and green show those measured by utilizing the temperatures of the PP and the He tank in orbit, with assumptions of the flight-model PP mass flow rate and two-thirds of that, respectively.[5] (b) The consumed He amount calculated by integrating the simulated He mass flow rate in panel (a). The initial amount of the LHe in the He tank was ~5162 g.

beginning-of-life cryocooler performance was estimated at ~4.7 years, which is ~0.2 years longer than that predicted by Yoshida et al.[7] before the launch. This is because the initial LHe amount was ~6% larger than they assumed (33.6 L). Note that cryocooler performance is expected to gradually degrade, making the IVCS and OVCS temperatures increase. The higher IVCS temperature provides the higher positive heat load from the DA to the He tank, making the He mass flow rate increase. This makes the LHe lifetime shorter, and hence, we also carried out the calculation with the end-of-life (EOL) performance of the cryocoolers, to obtain a lower lifetime limit. We replaced the negative heat loads at the first and second stages of the SCs in Table 2 by the EOL performances, $-28T_{\mathrm{SC\,first}} + 2885$ mW ($T_{\mathrm{SC\,first}} > 103$ K) and $-17T_{\mathrm{SC\,second}} + 260$ mW ($T_{\mathrm{SC\,second}} > 15$ K), respectively, and simulated the temperature distribution in equilibrium. In this case, the He mass flow rate was ~42 μg/s, giving a helium lifetime of ~3.9 years in the EOL case, which still satisfies the requirement of over 3 years. As a conclusion, the lifetime of the He vaporization cooling operation would be at least ~3.9 to 4.7 years, and the SXS cooling system was working well as designed in the orbit.

5 Conclusion

The cooling system of Hitomi/SXS utilizes the porous plug phase separator to separate liquid and boiloff helium under zero gravity, and to vent only the boiloff helium to space. Because the system works properly only when the superfluid phase exists, the LHe temperature must be kept under the λ point in orbit. Because the launch timeline involves periods of time in which there is no helium venting and the cryocoolers are turned off, the helium warms appreciably during the final launch operations and shortly into flight. In order to investigate the maximum allowable helium temperature at launch, we constructed a thermal mathematical model of the SXS dewar, which incorporated proper helium mass flow rate through the flight-model porous plug, and simulated temperature variations by changing the initial LHe temperature and the timing to start operations of SCs. The maximum allowable helium temperature was thus determined to be ~1.7 K at launch, and this value was utilized as a launch commit criteria. We also carried out a thermal calculation using the actual temperatures at the launch and confirmed that the helium temperature behavior was well reproduced by the thermal simulation. From the predicted helium mass flow rate, the lifetime of the helium mode was estimated at ~3.9 to 4.7 years, which satisfies the requirement of 3 years.

Disclosures

The authors have no relevant financial interests in the paper and no other potential conflicts of interest to disclose.

Acknowledgments

The authors are deeply grateful to all members of the Hitomi team and cryogenic group at the Niihama Division of Sumitomo Heavy Industries, Ltd. for their support. H.N. was supported by the Grant-in-Aid for Young Scientists (B) (26800095) from the Japan Society for the Promotion of Science and the Special Postdoctoral Researchers Program in RIKEN.

References

1. R. L. Kelley et al., "The Astro-H high resolution soft x-ray spectrometer," *Proc. SPIE* **9905**, 99050V (2016).
2. T. Takahashi et al., "The ASTRO-H (Hitomi) x-ray astronomy satellite," *Proc. SPIE* **9905**, 99050U (2016).
3. Hitomi Collaboration and F. Aharonian et al., "The quiescent intracluster medium in the core of the Perseus cluster," *Nature* **535**, 117–121 (2016).
4. R. Fujimoto et al., "Performance of the helium dewar and cryocoolers of ASTRO-H SXS," *Proc. SPIE* **9905**, 99053S (2016).
5. Y. Ezoe et al., "Porous plug phase separator and superfluid film flow suppression system for the soft x-ray spectrometer onboard ASTRO-H," *Proc. SPIE* **9905**, 99053P (2016).
6. Y. Ezoe et al., "Flight model measurements of the porous plug and film flow suppression system for the ASTRO-H soft x-ray spectrometer dewar," *Cryogenics* **74**, 17–23 (2016).
7. S. Yoshida et al., "Flight model performance test results of a helium dewar for the soft x-ray spectrometer onboard ASTRO-H," *Cryogenics* **74**, 10–16 (2016).
8. P. J. Shirron et al., "Design and on-orbit operation of the adiabatic demagnetization refrigerator on the Hitomi soft x-ray spectrometer instrument," *Proc. SPIE* **9905**, 99053O (2016).

9. K. Narasaki et al., "Development of two-stage Stirling cryocooler for ASTRO-F," *Adv. Cryog. Eng.* **49B**, 1428–1435 (2004).
10. K. Narasaki et al., "Development of cryogenic systems for SMILES," *Adv. Cryog. Eng.* **49B**, 1785–1794 (2004).
11. Y. Ezoe et al., "Development of porous plug phase separator and superfluid film flow suppression system for the soft x-ray spectrometer onboard ASTRO-H," *Cryogenics* **52**, 178–182 (2012).
12. R. J. Donnelly and C. F. Barenghi, "The observed properties of liquid helium at the saturated vapor pressure," *J. Phys. Chem. Ref. Data* **27**, 1217–1274 (1998).
13. M. Tsujimoto et al., "In-orbit operation of the ASTRO-H SXS," *Proc. SPIE* **9905**, 99050Y (2016).

Hirofumi Noda is an assistant professor at Tohoku University. He received his BS degree in astronomy from Tohoku University in 2009 and his MS and PhD degrees in astronomy from the University of Tokyo in 2011 and 2013, respectively. His current research interests include instrumentation of x-ray microcalorimeters and high-energy astrophysics, especially phenomena around supermassive black holes.

Biographies for the other authors are not available.